



Pergamon

Available online at [www.sciencedirect.com](http://www.sciencedirect.com)

SCIENCE @ DIRECT®

Acta Materialia 51 (2003) 3915–3926



[www.actamat-journals.com](http://www.actamat-journals.com)

# Identification of the segregation layer and its effects on the activated sintering and ductility of Ni-doped molybdenum

K.S. Hwang \*, H.S. Huang

*Department of Materials Science and Engineering, National Taiwan University, 1 Roosevelt Road, Sec. 4, Taipei, 106 Taiwan*

Received 29 December 2002; received in revised form 10 April 2003; accepted 11 April 2003

## Abstract

Previous literature has shown that the sintering temperature of molybdenum compacts can be decreased significantly through activated sintering by adding a small amount of nickel. This nickel doping, however, reduces the ductility of the material. A number of studies have postulated mechanisms to explain this enhanced sintering and embrittlement, but little direct evidence has been reported to date. In this study, the use of a field emission transmission electron microscope and a scanning Auger electron microscope has identified a  $\delta$ -NiMo intermetallic compound film, about 2 nm thick, at the grain boundaries. An experiment focusing on the Mo/Ni-Mo diffusion couple shows that the  $\delta$ -NiMo layer at the grain boundaries serves as a short-circuit diffusion path and causes the activated sintering of Ni-doped molybdenum. This compound is, however, intrinsically brittle and thus is the root cause of the embrittlement problem of Ni-doped molybdenum.

© 2003 Acta Materialia Inc. Published by Elsevier Science Ltd. All rights reserved.

*Keywords:* Sintering; Intermetallic compounds; Grain boundary embrittlement; Diffusion; Auger electron spectroscopy

## 1. Introduction

Small additions of group VIII B transition elements such as Ni, Pd, and Pt to tungsten and molybdenum effectively lower the activation energy of sintering for these refractory metals. The mechanism of such activated sintering has previously been investigated and reported [1–6]. In the case of molybdenum, it is generally believed that the molybdenum powder surface and the interpar-

ticle contact area are covered by a nickel, or nickel-rich, layer during sintering. Since molybdenum has a high diffusion rate and high solubility in nickel, while nickel has a very low diffusion rate and low solubility in molybdenum, the Mo-Ni system exhibits pronounced unipolar diffusion through the segregated layer and thus the activated sintering [1,4,7,8]. However, little detailed information has been provided on the segregated layer, and how this layer causes the activated sintering remains uncertain.

In addition to molybdenum and tungsten, activated sintering in oxides has also been reported. In the case of Bi<sub>2</sub>O<sub>3</sub>-doped ZnO sintered in the solid state, an amorphous film was detected at the grain

\* Corresponding author. Tel.: +886-223-633-126; fax: +886-223-634-562.

E-mail address: [kshwang@ccms.ntu.edu.tw](mailto:kshwang@ccms.ntu.edu.tw) (K.S. Hwang).

boundaries by Chiang et al., through the use of a high-resolution transmission electron microscope [9,10]. The enhanced sintering of ZnO is thus ascribed to the faster mass transport through the disordered amorphous film. With these findings, it is reasonable to suspect that an amorphous film might also be present during the activated sintering of the Ni-doped Mo. However, an examination of this possibility has yet to be conducted.

Though the addition of nickel enhances the sintering of molybdenum, this benefit comes at a cost, namely brittleness of the sintered parts, thus making subsequent thermo-mechanical processing impossible [11–13]. As the exact mechanism of the activated sintering has not been established, the mechanism of the embrittlement is not well understood either. It is generally accepted that the nickel segregations at the grain boundaries are related to the poor ductility of sintered Mo compacts [12–15]. It has been postulated that intermetallic compounds could be the cause of this embrittlement. Mil'man et al., using an x-ray diffractometer, showed that  $\delta$ -NiMo compounds were present in sintered Mo compacts containing 1–20 wt% Ni. However, these sites, at the grain junctions or at the boundaries, have not been identified. More recently,  $\delta$ -NiMo compound clusters were detected at grain junctions in Mo-Ni and Mo-Ni-Al compacts [14,15]. The NiMo and Ni<sub>3</sub>Mo compounds were also found by Chou and Link at the interface between the stacked Mo and Ni discs [16]. In addition to the intermetallic compounds, the cause of the embrittlement by the formation of glassy phases at the grain boundaries, as was found by Chiang et al., cannot be ruled out either [9,10]. These previous studies, while having provided some insights on the embrittlement mechanism, direct observations and the nature of the segregated layer at the grain boundaries, have not been reported as of yet.

The segregated layer in the Mo-Ni system, whatever it may be, must play an important role in the enhanced sintering and the embrittlement. This paper presents direct evidence for the presence of the segregated layer at the grain boundaries of the Ni-doped molybdenum. Its chemical composition and the structure are identified. The intrinsic properties and diffusion data of this segregated

phase are also investigated and are used to explain why the activated sintering and the embrittlement occur.

## 2. Experimental procedure

Fine molybdenum powder and fine nickel powder were selected as the base materials for this study. The characteristics of the two powders, including chemistry, are given in Table 1.

To prepare the compacts, molybdenum powder was mixed with different amounts of nickel powder for 1 h and then pressed into 65% dense rectangular bars, 40 × 15 × 4.3 mm, using a pressure of 450 MPa. The green compacts were heated at a rate of 10 °C/min and then held at 1300 °C for 1 h in hydrogen. For comparison, a pure molybdenum standard was prepared by pressing and sintering pure molybdenum powders, using the same conditions, except that the final sintering was carried out at 1750 °C for 20 hs under vacuum. For the transmission electron microscope (TEM) analysis, the specimen was quenched in water after sintering so that the structure existing at high temperatures could be preserved. To understand the effect of nickel on the sintering of molybdenum, a thermal dilatometer (TMA16/18, Setram Co., Caluire, France) was employed to monitor the phase changes and the shrinkage during sintering.

The sintered densities were measured by the Archimedes' method. To examine the transverse

Table 1  
Characteristics of the Mo and Ni powders used in this study

Powder	Mo	Ni
Designation	OMP 901	Ni-123
Particle size (laser scattering), $\mu\text{m}$		
D <sub>10</sub>	1.0	2.3
D <sub>50</sub>	2.5	3.6
D <sub>90</sub>	5.8	6.9
Pycnometer density, $\text{g}/\text{cm}^3$	10.18	8.89
Chemistry, %		
C	0.0019	0.0808
O	0.9268	0.1955
N	0.0088	0.0015
Supplier	H.C. Starck	INCO

rupture strength, specimens were ruptured by the 4-point bending test at a crosshead speed of 2.5 mm/min. The hardness was measured by a Vickers microhardness tester (MVK-E2, Akashi Co., Tokyo, Japan) using a 50 g load. The grain size was determined by the line-intercept method from micrographs taken by the scanning electron microscope (SEM, XL30, Philips Co., Eindhoven, Holland). For chemical analysis, an electron probe microanalyzer (EPMA, JXA-8600SX, JEOL Co., Tokyo, Japan) was used to examine the nickel distribution. To examine the composition of the segregation at the grain boundaries, sintered specimens were fractured inside a scanning Auger electron microscope (SAM, 660, Perkin Elmer Co., Minnesota, USA) under a high vacuum of  $5.3 \times 10^{-8}$  Pa, so that the ruptured surfaces were not contaminated. The depth profile of the segregated layer was determined using the argon ion sputtering method. The sputtering rate was 1 nm/min with reference to a Ta<sub>2</sub>O<sub>5</sub> standard. The structure of the segregated layer was further examined using a field emission transmission electron microscope (FETEM, TECNAI F30, Philips Co., Eindhoven, Holland) with a voltage of 300 kV.

Previous studies have shown that  $\delta$ -NiMo compounds formed easily in the Ni-Mo system [7,13–16]. A NiMo compound in the bulk form was thus prepared for use in the identification of the materials being examined. To prepare this standard, the mixed powder of 50 at% Ni and 50 at% Mo was pressed and then sintered at 1300 °C for 1 h in hydrogen. The sintered compact was melted in an arc-melting furnace under a vacuum  $1.3 \times 10^{-2}$  Pa. The resulting microstructure in the as-cast specimen was dendritic, and the specimen was thus further annealed at 1300 °C for 100 hs to obtain a homogeneous microstructure with equiaxed grains. The final chemical composition of this compound was Ni-49.44 at% Mo, as was measured by the EPMA.

To understand the interdiffusion behavior between molybdenum and nickel, a diffusion couple consisting of pure Mo and a solid solution of Ni-17 at% (25 wt%) Mo was prepared. Before diffusion began, 0.3  $\mu$ m zirconia particles were sprinkled on the interface as the interface markers. The diffusion couple was annealed at 1280 °C for

different lengths of time. The calculation of the interdiffusion coefficient  $\bar{D}$  was based on the method proposed by Wagner [17]. The intrinsic diffusion coefficients,  $D_{\text{Ni}}$  and  $D_{\text{Mo}}$ , at the marker interface were determined using two methods proposed by Darken and Heumann, respectively [18–21].

### 3. Results

#### 3.1. Sintered properties

Fig. 1(a) and (b) show, respectively, the amount of shrinkage and the shrinkage rate of the Mo compacts with and without the Ni additions. It is illustrated that the sintering was significantly enhanced even when only 0.5 wt% Ni was added. The amount of shrinkage increased from 1.5% for the pure Mo to 8.1% when the temperature reached 1300 °C. No abrupt changes in either the dimensions or the shrinkage rate curves were noticed at the eutectic temperature of 1317 °C, nor at the peritectic temperature of 1362 °C [22]. This suggested that the entire 0.5 wt% Ni was dissolved into the Mo matrix and thus the sintering proceeded in the solid state throughout the heating period. As the amount of Ni increased to 1.5 and 3 wt%, the slope of the sintering curves changed at 1362 °C. This change is clearly shown in Fig. 1(b), which illustrates the shrinkage rate curves. These results and the Mo-Ni phase diagram suggested that when 1.5 wt% and 3.0 wt% Ni were added, some Ni dissolved into the Mo, while the rest formed  $\delta$ -NiMo compounds and caused the peritectic reaction,  $\delta$ -NiMo $\leftrightarrow$ L+Mo. Since no eutectic reaction (Ni+ $\delta$ -NiMo $\leftrightarrow$ L) occurred at 1317 °C, there must have been very little, if any, free nickel or Ni-rich solid solution present in the compact.

Since this study focused on activated sintering, the following experiments were performed at 1300 °C in the solid state. The amount of Ni added was fixed at 1.5 wt% (2.4 at%). Table 2 shows that 95.5% density was attained on the Mo-1.5 wt% Ni compact. In contrast, the pure molybdenum compact only sintered to 82.1%. The hardnesses were HV310 and HV110 for the Mo-1.5 wt% Ni and pure molybdenum, respectively. Despite the high

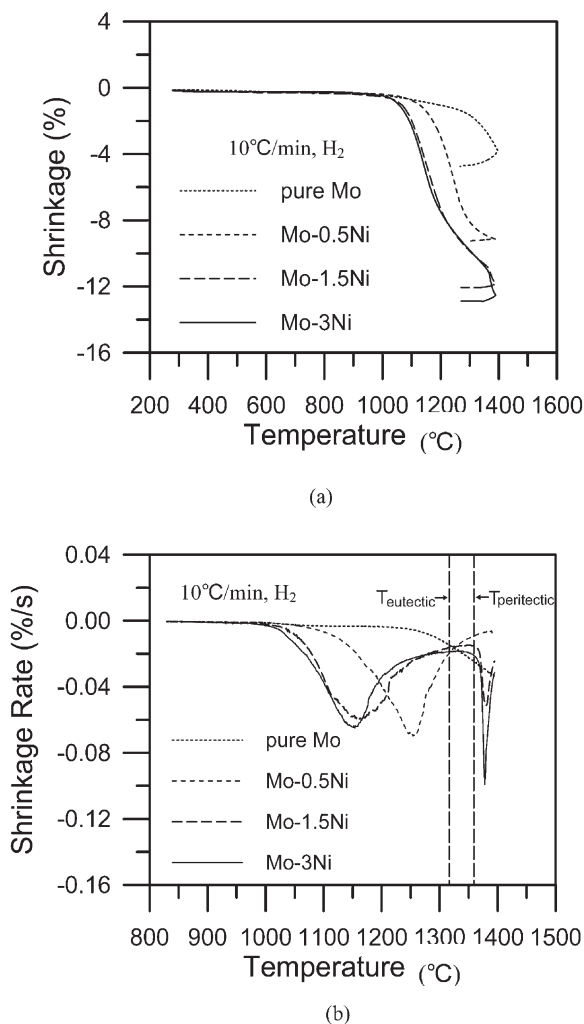


Fig. 1. (a) The dilatometer curves and (b) their derivatives of Mo compacts with Ni additions.

Table 2

The density, hardness, and bending strength of Mo and Mo-1.5 wt% Ni compacts sintered at 1300 °C for 1 h

	Density, %	Hardness, HV	Bending strength, MPa
Mo	82.1	110	605
Mo-1.5 wt% Ni	95.5	310	340

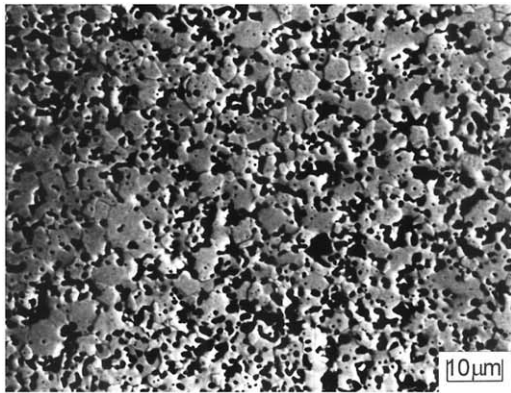
sintered density and high hardness, the bending strength of the Mo-1.5 wt% Ni compacts was only 340 MPa, lower than the 605 MPa of the 82.1% dense pure Mo compact. No signs of ductility were noticed at the fracture surfaces in either the Mo-1.5 wt% Ni or the 82.1% dense pure Mo compacts.

### 3.2. Microstructure and chemical analysis

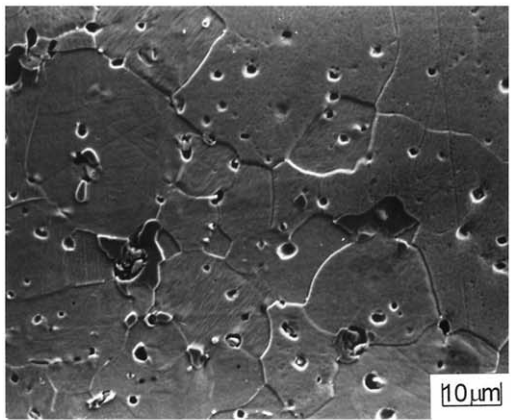
To understand the causes of the enhanced densification and the poor ductility of Ni-doped Mo, analytical instruments were employed to examine the microstructure and the chemical composition in detail. Fig. 2 compares the microstructures of the Mo-1.5 wt% Ni and the pure Mo compacts that were sintered at 1300 °C. The grain size shown in Fig. 2(a), that of the 82.1% dense Mo, was smaller than that shown in Fig. 2(b), that of the Mo-1.5 wt% Ni. The X-ray mapping of the Mo-1.5 wt% Ni compact shown in Fig. 2(c) illustrates that some nickel-rich areas were present at the grain junctions. The EPMA analysis revealed that the ratio of the Mo to Ni in these clusters was close to 1. The energy dispersive spectrum (EDS) and the electron diffraction pattern shown in Fig. 3 further confirmed that these clusters were  $\delta$ -NiMo, not a Ni-rich solid solution.

In order to understand whether the  $\delta$ -NiMo compound was also segregated at the grain boundaries, a quenched Mo-1.5 wt% Ni compact was ruptured inside the scanning Auger microscope so that fracture surface analysis could be conducted. Fig. 4 shows that all fracture surfaces were of the intergranular type. The Auger spectrum of the area No. 1 in Fig. 4 further illustrates that a high concentration of nickel was present, as depicted in Fig. 5(a). Examination of other areas also showed similar spectra.

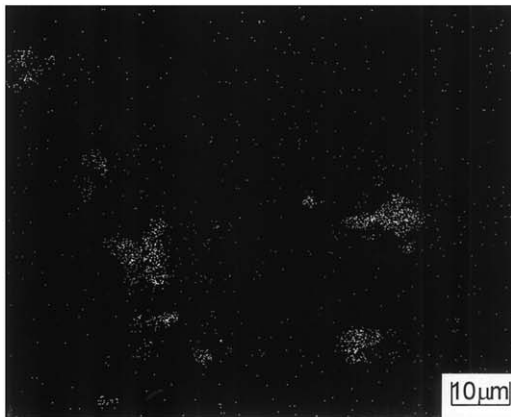
To estimate the thickness of this nickel-containing layer, the argon sputtering method, with a sputtering rate of 1 nm/min, was employed. Fig. 5(b) shows that, after 60 seconds of sputtering, the nickel peaks disappeared. This suggested that the thickness of the layer examined was about 1 nm. Considering that nickel was detected on both sides of the fractured specimen, the total thickness of this nickel-rich phase was about 2 nm prior to fracturing.



(a)

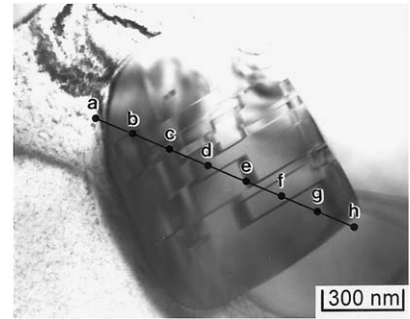


(b)

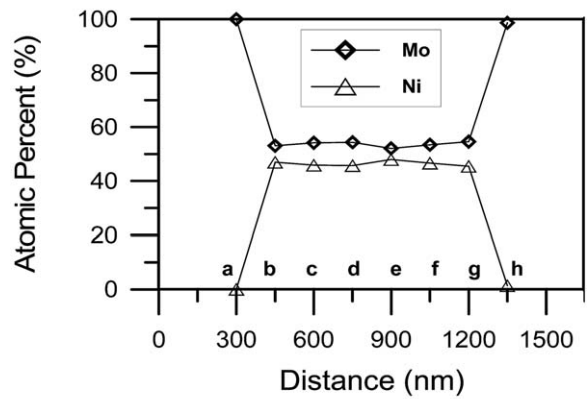


(c)

Fig. 2. The microstructures of (a) Mo and (b) Mo-1.5 wt% Ni compacts sintered at 1300 °C for 1 h. (c) The nickel distribution in the Mo-1.5 wt% Ni compact shown in (b).



(a)



(b)



(c)

Fig. 3. Phase identification of the  $\delta$ -NiMo intermetallic compound at the grain junctions in Mo-1.5 wt% Ni sintered compacts. (a) TEM bright field image, (b) chemical analysis by EDS, (c) electron diffraction pattern.

To identify the composition of this layer, further Auger analysis was employed using a bulk  $\delta$ -NiMo intermetallic compound as the standard. Fig. 6 shows that the average nickel content at the surface layer was 35.46 at%. A similar finding of 15 at% Ni was also reported by Hofmann et al., on sintered

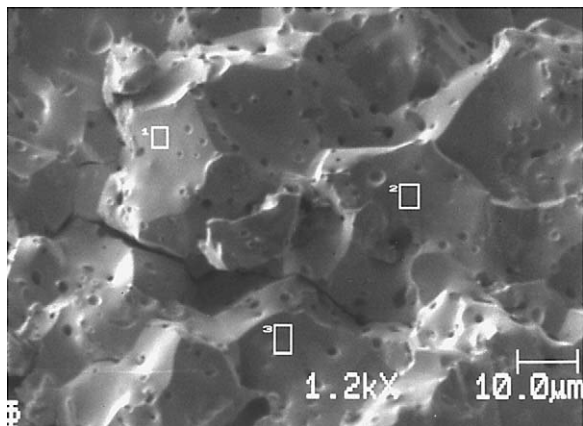


Fig. 4. The rupture surfaces of Mo-1.5 wt% Ni compacts sintered at 1300 °C showing the intergranular type of fracture. Areas 1, 2, and 3 were randomly selected for the Auger analysis.

Mo-1 wt% Ni compacts [12]. Since a compound with these nickel contents cannot be found in the Mo-Ni phase diagram, it is reasonable to suspect that Mo signals were picked up from the regions below the thin  $\delta$ -NiMo layer, thus causing the low reading for Ni. It is also possible that this Mo-35.46 at% Ni was in the amorphous form, similar to the findings reported in the literature for activation-sintered Bi<sub>2</sub>O<sub>3</sub>-ZnO system [9,10]. A FETEM was thus used to examine the lattice structure near the grain boundaries. Fig. 7 illustrates that a crystalline, not amorphous, film was present at the grain boundaries. The lattice spacing of this film was 0.221 nm and the thickness of this layer was about 2 nm, consistent with the depth profile result obtained by the previous Auger analysis. The EDS of the segregated layer, as shown in Fig. 8, again confirmed that this layer was enriched with nickel. These results rule out the possibility that the densification is caused by the fast diffusion through the glassy phase at the grain boundaries.

Based on the previous SAM, EPMA, and FETEM analyses, it is logical to conclude that the thin layer at the grain boundaries is the  $\delta$ -NiMo compound. In order to understand the influence of this compound on the ductility, we next examined the intrinsic properties of the vacuum-cast  $\delta$ -NiMo compound. The hardness measured was HV992 and the coefficient of thermal expansion (CTE)

was  $7.96 \times 10^{-6}$ , as shown in Table 3 along with the density and the resistivity. It was noticed during the hardness testing that the  $\delta$ -NiMo compound was extremely brittle, as was indicated by the cracks at the diagonals of the indentation marks, as shown in Fig. 9.

### 3.3. Interdiffusion behavior of Mo-Ni

To help explain the activation effect during the sintering of nickel-added molybdenum, Mo and Ni discs were stacked and annealed at 1280 °C for up to 100 hs. Only the  $\delta$ -NiMo phase, and no other intermetallic compound, was found at the Mo-Ni interfaces. It was originally intended that the concentration data obtained from this Mo-Ni diffusion couple be used for the calculation of the diffusion coefficients. However, it was found that the marker interface was outside the compound layer, which makes the calculation difficult. A second diffusion couple was thus prepared by using a Mo/Ni-17 at% (25 wt%) Mo. Fig. 10(a) shows the cross-section of the sample annealed for 25 hs at 1280 °C. Its concentration-penetration profile, as shown in Fig. 10(b), revealed that the ZrO<sub>2</sub> marker interface was located within and at the left side of the  $\delta$ -NiMo compound layer. This allows the interdiffusion coefficient  $\tilde{D}$  and intrinsic diffusion coefficients  $D_{Ni}$  and  $D_{Mo}$  at the ZrO<sub>2</sub> marker interface to be determined using the Darken equation based on the Boltzmann-Matano analysis [18,19]. Table 4 shows that the interdiffusion coefficient  $\tilde{D}$  at 1280 °C is  $3.22 \times 10^{-10}$  cm<sup>2</sup>/sec. This is in good agreement with the  $2.8 \times 10^{-10}$  cm<sup>2</sup>/sec and  $3.0 \times 10^{-10}$  cm<sup>2</sup>/sec rates reported by Hweiwegen and Rieck, who used Ni/Ni-58.8 at% Mo and Mo/Ni-38 at% Mo diffusion couples, respectively [7].

Based on the Darken equation, the calculated  $D_{Mo}$  and  $D_{Ni}$  in the  $\delta$ -NiMo at the marker interface were  $3.22 \times 10^{-10}$  cm<sup>2</sup>/sec and  $3.24 \times 10^{-10}$  cm<sup>2</sup>/sec, respectively. The  $D_{Ni}/D_{Mo}$  ratio also agrees with the ratio of 0.9 that was measured by Hweiwegen and Rieck using the Mo/Ni-38 at% Mo annealed for 20 hs at 1275 °C [7]. This ratio was not surprising because the Matano interface was very close to the ZrO<sub>2</sub> marker interface, suggesting that the diffusion rates of molybdenum and nickel at the marker interface are almost equal. When

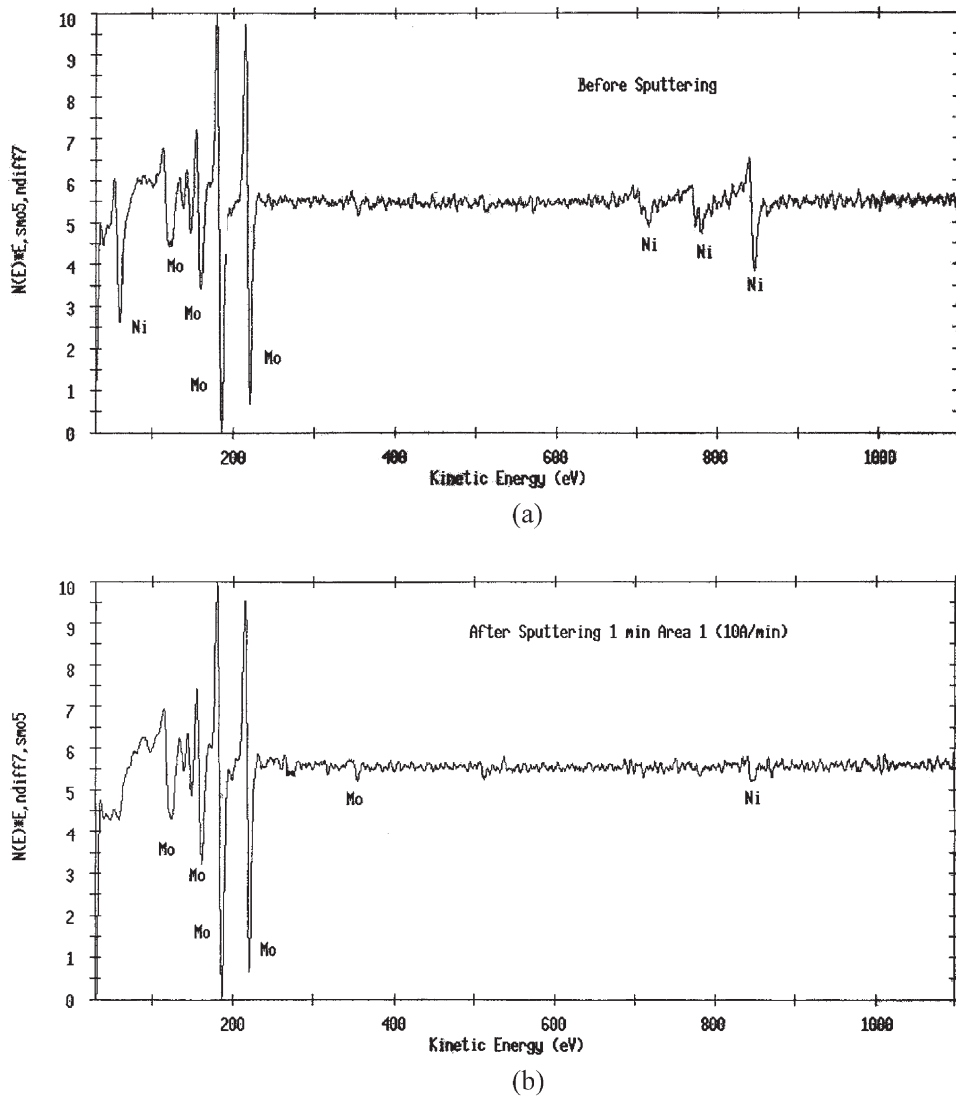


Fig. 5. The Auger spectra of the surface No. 1 shown in Fig. 4. (a) Before sputtering, (b) after sputtering for 1 min.

Heumann's equation was used, the  $D_{\text{Mo}}$  and  $D_{\text{Ni}}$  were  $2.76 \times 10^{-10}$   $\text{cm}^2/\text{sec}$  and  $3.56 \times 10^{-10}$   $\text{cm}^2/\text{sec}$ , respectively [20].

## 4. Discussion

### 4.1. Identification of the segregated layer

Previous literature has suggested that the segregation layer of the activation-sintered molybdenum

could be a Ni or Ni-containing layer [4,12,15]. The results from the dilatometer experiments and the Mo-Ni phase diagram suggest that these layers did not contain pure Ni or Ni-rich solid solutions because no eutectic reaction was noticed during heating. The FETEM image, shown in Fig. 7, further indicates that this Ni-rich segregation is a crystalline layer with the lattice spacing of 0.221 nm. This is greater than the largest interplanar spacing of nickel, which is 0.2034 nm for the (111) plane. It could be argued that the dissolution of

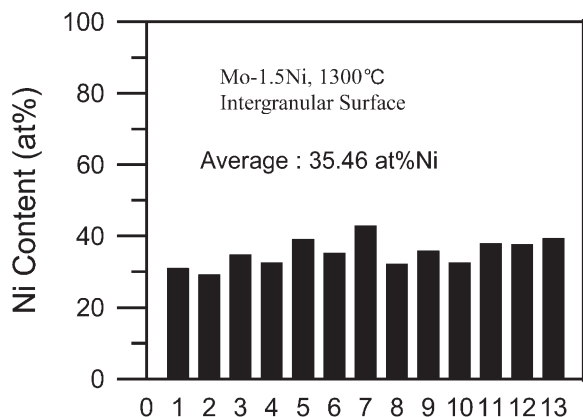


Fig. 6. The amount of Ni in the Ni-rich layer of the Mo-1.5 wt% Ni compact sintered at 1300 °C.

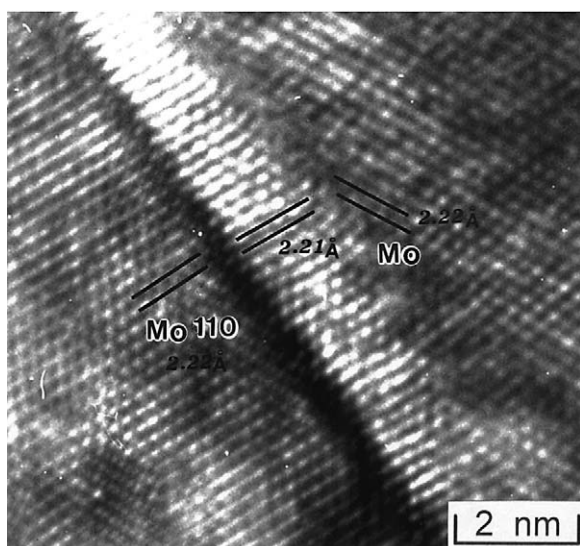


Fig. 7. The high-resolution lattice fringe of the grain boundaries in quenched Mo-1.5 wt% Ni compacts.

Table 3  
The measured properties of the  $\delta$ -NiMo intermetallic compound

Material	$\delta$ -NiMo
Composition	Ni-49.44 at% Mo
Density ( $\text{g}/\text{cm}^3$ )	9.78
Hardness ( $\text{HV}_{200}$ )	992
Electrical resistivity ( $\Omega\cdot\text{cm}$ )	$9.90 \times 10^{-5}$
Thermal expansion ( $\text{mm}/\text{mm}\cdot^\circ\text{C}$ )	$7.96 \times 10^{-6}$

molybdenum into nickel may expand nickel's lattice parameter. The spacing of plane (111) of the nickel solid solution calculated with the largest amount of molybdenum soluble, 27.5 at% Mo, is 0.21 nm. This is still far below 0.221 nm [22]. Thus, the segregated layer is neither pure nickel nor a nickel solid solution.

Table 5 compares the lattice spacings of the planes, which are close to 0.221 nm in Mo, Ni, NiMo, Ni<sub>3</sub>Mo, and Ni<sub>4</sub>Mo. Although Ni<sub>3</sub>Mo show a lattice parameter of 0.222 nm for an unidentified plane, this compound was never found in the diffusion couple or by EPMA analysis. Thus, based on these results, the most likely phase of the nickel-rich layer is the NiMo compound. This agrees with the dilatometry results shown in Fig. 1, which indicate that no eutectic reaction occurred at 1317 °C during heating. Only the peritectic reaction at 1362 °C was observed.

#### 4.2. Mechanism of embrittlement

The experiments described above show that a Ni-doped Mo compact has low strength and no ductility. Previous literature has shown that grain coarsening occurs during activated sintering and could be one of the factors causing the brittle fracture [11,12,23]. This study also observed large grain sizes averaging 26.9  $\mu\text{m}$  in the Mo-1.5 wt% Ni compacts sintered at 1300 °C for 1 h. Our previous study [24] showed that pure Mo, when sintered at 1750 °C to the same 95.5% density, has a grain size of 72  $\mu\text{m}$  yet retains good ductility. This indicates that the grain coarsening that occurred in the activated sintering is not the main factor causing the embrittlement.

The more likely cause of the embrittlement is the intrinsic brittleness of the  $\delta$ -NiMo compound at the grain boundaries, as was observed by the cracks at the tips of the indentation marks in the bulk  $\delta$ -NiMo compound. Since the Auger analysis indicated that nickel was detected on all fractured surfaces, the brittle fracture must occur within the thin  $\delta$ -NiMo layer, not at the interface between the compound and the molybdenum matrix. Furthermore, the mismatch in the thermal expansion coefficient (CTE) between the segregated  $\delta$ -NiMo compound and the Mo matrix may also aggravate the

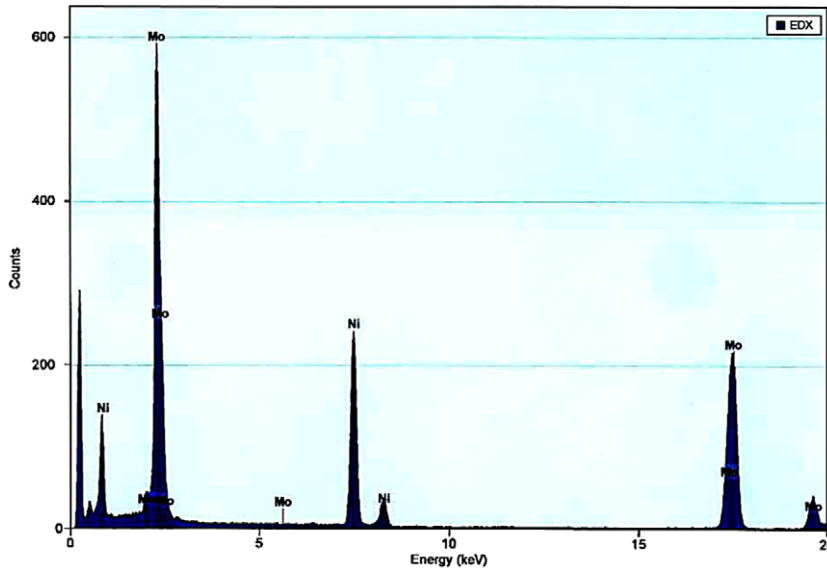


Fig. 8. The EDS spectrum showing a high concentration of nickel at the boundaries between the Mo grains.

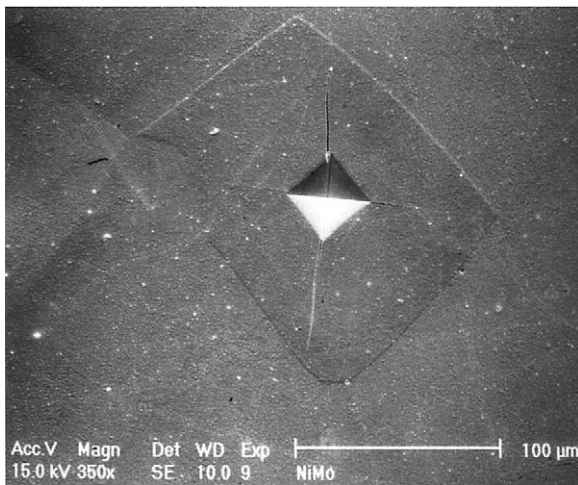
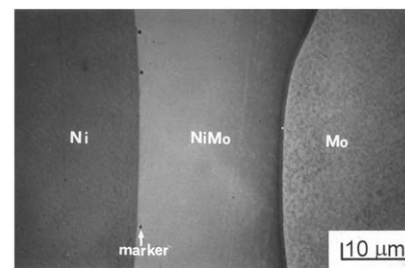
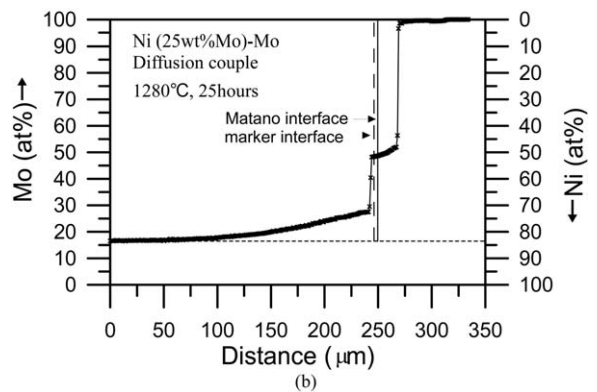


Fig. 9. Cracks at the tips of the diamond indentation mark showing that the NiMo compound is a very brittle material.

problem with ductility. Table 3 shows that the CTE of the compound is  $7.96 \times 10^{-6}$  mm/mm-°C, which is much higher than the  $5.2 \times 10^{-6}$  mm/mm-°C of the Mo. This mismatch might cause micro cracks at the grain boundaries of the sintered compact during cooling.



(a)



(b)

Fig. 10. The diffusion couple of Mo-Ni(17 at% Mo) annealed at 1280 °C for 25 hs. (a) the microstructure of the cross-section, and (b) the concentration profile.

Table 4

The diffusion coefficients in the  $\delta$ -NiMo at the marker interface determined from the Mo/Ni-17 at% Mo diffusion couple annealed at 1280 °C for 25 hs

Interdiffusion coefficient, $\bar{D}$ (cm <sup>2</sup> /sec)	Intrinsic diffusion coefficient	
	$D_{\text{Mo}}$ (cm <sup>2</sup> /sec)	$D_{\text{Ni}}$ (cm <sup>2</sup> /sec)
$3.22 \times 10^{-10}$	$3.22 \times 10^{-10}$	$3.24 \times 10^{-10}$
	(Darken eq.)	$3.56 \times 10^{-10}$
	$2.76 \times 10^{-10}$	
	(Heumann eq.)	

#### 4.3. Mechanism of activated sintering

Previous literature [1–7] has suggested that the activated densification is caused by the fast mass transport of molybdenum atoms through the nickel, or nickel-rich, layer between molybdenum particles. This study, however, did not produce any evidence of the presence of nickel or nickel solution layers. It was very likely that the disappearance of nickel was caused by the slow heating rate of 10 °C/min, which provided enough time for the nickel to dissolve into the Mo matrix or to react with the Mo to form the  $\delta$ -NiMo compound. To reduce the heating time, a dilatometer experiment using a heating rate of 99 °C/min from room temperature to 1280 °C was employed. The heating rate was then switched to 10 °C/min from 1280–1400 °C to avoid temperature overshooting and to facilitate the taking of accurate temperature readings. With this heating profile, no eutectic reaction was detected by the dilatometer either. Only the peritectic reaction was observed. This suggests that the  $\delta$ -NiMo compound formation is extremely fast

and is difficult to avoid, even with a fast heating rate. Thus, the enhanced sintering must be related to the formation of this  $\delta$ -NiMo compound layer, not nickel.

Table 4 further shows that the diffusivity of Mo in the  $\delta$ -NiMo compound at 1280 °C is about  $3 \times 10^{-10}$  cm<sup>2</sup>/sec, which is about 26,000 times higher than that of the self diffusion of pure molybdenum,  $1.15 \times 10^{-14}$  cm<sup>2</sup>/sec [25]. Based on the findings on the thin  $\delta$ -NiMo layer at the grain boundaries and the fast diffusion rate of Mo in this compound, the activation mechanism of the Ni-doped molybdenum can be described as follows. Fig. 11 illustrates that in the early stage of the sintering, nickel atoms quickly diffuse to the nearby areas and react with Mo, forming the  $\delta$ -NiMo intermetallic compound layers. This compound is very stable and does not dissolve into the Mo matrix. Thus, they are present at the contact areas between the Mo particles throughout the sintering. Since the diffusion rate of Mo in this compound is about 26,000 times that of its self-diffusion coefficient, these layers provide a fast diffusion path for the Mo atoms to diffuse to the neck areas, causing enhanced densification.

## 5. Conclusions

The embrittlement behavior and the activated sintering phenomenon of the Ni-doped molybdenum were investigated in this study. The results show that grain coarsening is not the cause of the poor ductility. It is not caused by the pure nickel, or nickel solid solution, layers at the grain bound-

Table 5

The intensities and lattice spacings of the planes which are close to 0.221 nm in the JCPDS data of Mo(42-1120), Ni(04-0850), NiMo(47-1129), Ni<sub>3</sub>Mo(17-0572), and Ni<sub>4</sub>Mo(03-1036)

Mo	Ni	NiMo	Ni <sub>3</sub> Mo	Ni <sub>4</sub> Mo
d (nm)(hkl), Int.	d (nm)(hkl), Int.	d (nm)(hkl), Int.	d (nm)(hkl), Int.	d (nm)(hkl), Int.
0.2224(110), 100	0.2034(111), 100	0.2420(132), 17	0.2527(200), 5	0.2803, 40
0.1574(200), 16	0.1762(200), 42	0.2220(401), 8	0.2224(002), 20	0.2052, 100
0.1574(200), 16	0.1246(220), 21	0.2210(004), 50	0.2220, 50	0.1996, 40
		0.2200(232), 23	0.2112(020), 80	0.1793(310), 90
		0.2150(141), 33	0.2035(102), 5	0.1763, 90

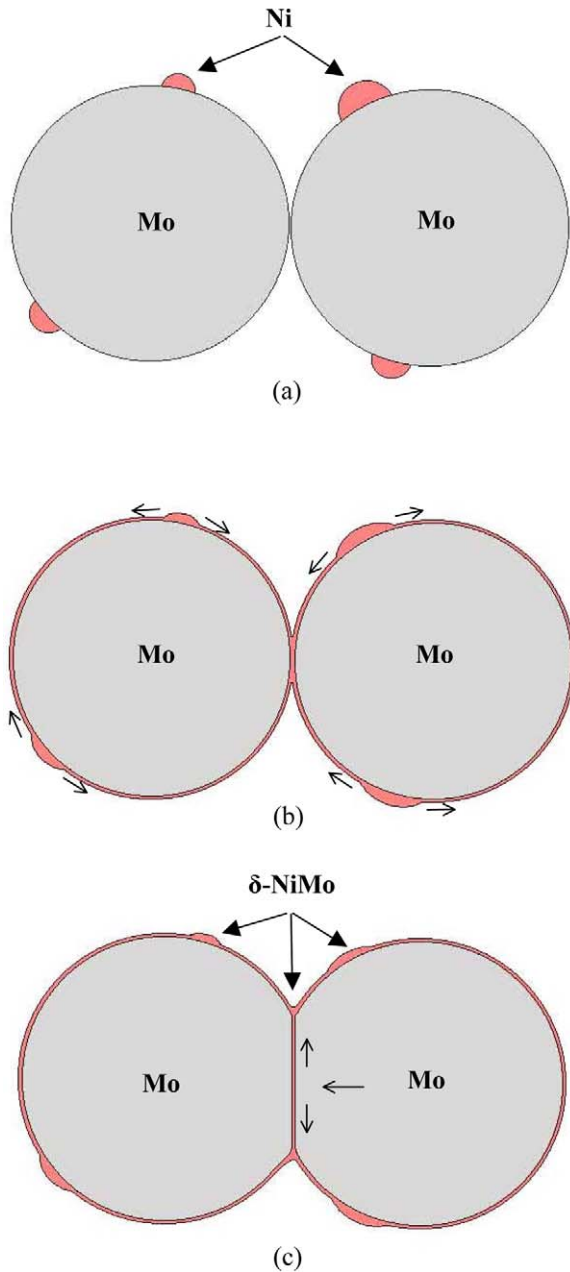


Fig. 11. Schematics of the activated sintering of Ni-doped molybdenum: (a) as-mixed, (b) Ni spreads over the Mo surface, (c) Mo transport through the  $\delta$ -NiMo compound layer to the neck.

aries, either. Instead, the brittle intermetallic compounds at the grain boundaries are responsible. This compound is identified as  $\delta$ -NiMo through field emission transmission electron microscope and the dilatometer analysis. The Auger analysis indicates that this  $\delta$ -NiMo compound layer covers all grain boundaries and is about 2 nm thick, as determined by the depth profile method and the FETEM analysis.

The diffusion studies show that the diffusion rate of Mo atoms in this  $\delta$ -NiMo compound is about 26,000 times that of its self-diffusion rate. This layer thus provides a short-circuit diffusion path and causes the activated sintering of the Ni-doped molybdenum.

### Acknowledgements

The authors wish to thank the National Science Council of the Republic of China for their support of this work under contract number NSC 90-2216-E-002-042. The supply of the molybdenum powder from H.C. Starck Inc. is also gratefully acknowledged.

### References

- [1] German RM, Munir ZA. Activated sintering of refractory metals by transition metal additions. *Rev Powder Metall Phys Ceram* 1982;2:9–43.
- [2] Brophy JH, Hayden HW, Wulff J. The sintering and strength of coated and co-reduced nickel tungsten powder. *Trans Metall Soc AIME* 1961;221:1225–31.
- [3] Hayden HW, Brophy JH. The activated sintering of tungsten with group VIII elements. *J Electrochemical Soc* 1963;110:805–10.
- [4] Smith JT. Diffusion mechanism for the nickel-activated sintering of molybdenum. *J Appl Phys* 1965;36:595–8.
- [5] Zovas PE, German RM, Hwang KS, Li CJ. Activated and liquid phase sintering—progress and problems. *J Metals* 1983;35:28–33.
- [6] Panichkina VV, Skorokhod VV, Khrienko AF. Activated sintering of tungsten and molybdenum powders. *Soviet Powder Metall and Phys Ceram* 1967;6:558–60.
- [7] Heijwegen CP, Rieck GD. Diffusion in the Mo-Ni, Mo-Fe and Mo-Co systems. *Acta Metall* 1974;22:1269–81.
- [8] Swalin RA, Martin A, Olsen R. Diffusion of magnesium, silicon, and molybdenum in nickel. *J Metals* 1957;9:936–9.

- [9] Wang H, Chiang Y-M. Thermodynamic stability of intergranular amorphous films in bismuth-doped zinc oxide. *J Am Ceram Soc* 1998;81:89–96.
- [10] Luo J, Wang H, Chiang YM. Origin of solid-state activated sintering in  $\text{Bi}_2\text{O}_3$ -doped ZnO. *J Am Ceram Soc* 1999;82:916–20.
- [11] Zovas PE, German RM. Retarded grain boundary mobility in activated sintered molybdenum. *Metall Trans A* 1984;15:1103–10.
- [12] Hofmann H, Grosskopf M, Hofmann-Antenbrink M, Petzow G. Sintering behavior and mechanical properties of activated sintered molybdenum. *Powder Metall* 1986;29:201–6.
- [13] Mil'man YV, Ristic MM, Gridneva IV, Lotsko DV, Kristanovich I, Goncharuk VA. Structure and hardness of sintered Mo-Ni alloys. *Soviet Powder Metall and Metal Ceram* 1987;26(2):144–8.
- [14] Hwang KS, Huang HS. The liquid phase sintering of molybdenum with Ni and Cu additions. *Mater Chem and Phys* 2001;67:92–100.
- [15] Sakamoto T, Nishida M, Okazaki K. Microstructure of Mo powders sintered with Ni and  $\text{Ni}_3\text{Al}$  powders. *J Jap Soc Powder Metall* 1999;46:1221–5.
- [16] Chou TC, Link L. Solid-state interdiffusion in Ni-Mo diffusion couples at high temperatures. *Scripta Mater* 1996;34:831–8.
- [17] Wagner C. The evaluation of data obtained with diffusion couples of binary single-phase and multiphase systems. *Acta Metall* 1969;17:99–107.
- [18] Darken LS. *Trans TMS-AIME* 1948;175:184.
- [19] Schmalzried H. *Solid state reactions*. 2nd ed. Weinheim: Verlag Chemie, 1981.
- [20] Heumann Th. *Z Phys Chem* 1952;201:168.
- [21] Ruth V, Powell GW. Concerning the determination of intrinsic diffusion coefficients in binary systems. *Acta Metall* 1964;12:264–7.
- [22] Singleton MF, Nash P. Mo-Ni (Molybdenum-Nickel). In: Nash P, editor. *Monograph series on alloy phase diagrams*. Phase diagram of binary nickel alloys, vol. 6. Materials Park, Ohio: ASM International; 1991. p. 207.
- [23] Li C, German RM. The properties of tungsten processed by chemically activated sintering. *Metall Trans A* 1983;14:2031–41.
- [24] Huang HS, Hwang KS. Deoxidation of molybdenum during vacuum sintering. *Metall and Mater Trans A* 2002;33:657–64.
- [25] Askill J. *Tracer diffusion data for metals, alloys, and simple oxides*. New York (NY): Plenum Press, 1970.